EQUIVARIANT DEEP EQUILIBRIUM MODELS FOR IMAGING INVERSE PROBLEMS

Alexander Mehta
University of California,
Berkeley
alexmehta@berkeley.edu

Ruangrawee Kitichotkul and
Vivek K Goyal

Boston University
{rkitich, goyal}@bu.edu

Julián Tachella CNRS & ENS Lyon julian.tachella@cnrs.fr

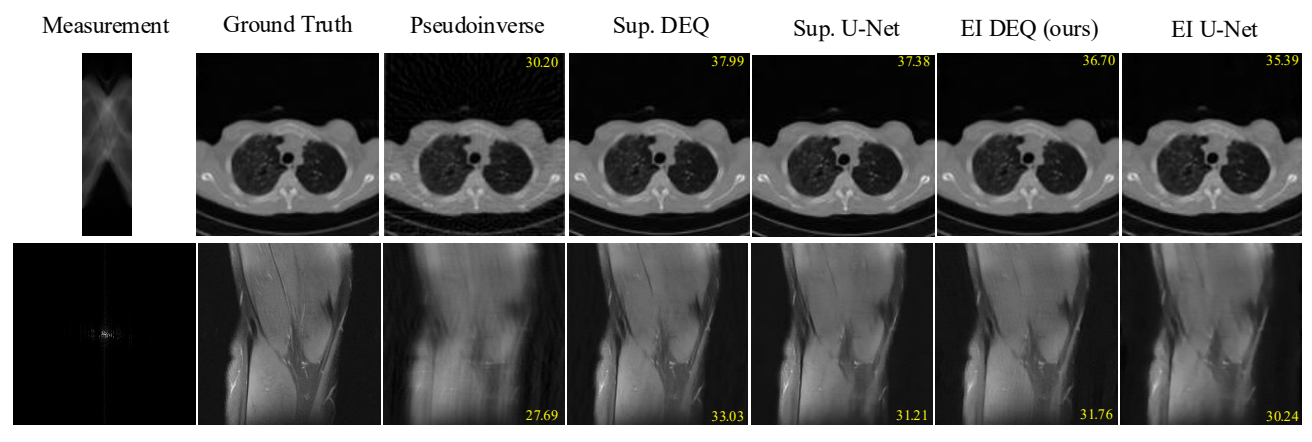


Fig. 1. Reconstructions from Deep Equilibrium Models (DEQs) and U-Nets trained with full supervision (Sup.) and without ground truth via equivariant imaging (EI). **Top –** Sparse View CT; **Bottom –** 8x Accelerated MRI with Noise. PSNR is reported in image corners.

ABSTRACT

Equivariant imaging (EI) enables training signal reconstruction models without requiring ground truth data by leveraging signal symmetries. Deep equilibrium models (DEQs) are a powerful class of neural networks where the output is a fixed point of a learned operator. However, training DEQs with complex EI losses requires implicit differentiation through fixed-point computations, whose implementation can be challenging. We show that backpropagation can be implemented modularly, simplifying training. Experiments demonstrate that DEQs trained with implicit differentiation outperform those trained with Jacobian-free backpropagation and other baseline methods. Additionally, we find evidence that EI-trained DEQs approximate the proximal map of an invariant prior.

Index Terms— Inverse Problems, Deep Equilibrium Models, Equivariant Imaging, Computational Imaging

1 INTRODUCTION

Many problems in signal processing can be formulated as inverse problems, where the goal is to recover the signal $x \in \mathbb{R}^n$ from the measurement $y \in \mathbb{R}^m$ under the forward model

$$y = Ax + \epsilon, \tag{1}$$

where $A:\mathbb{R}^n\to\mathbb{R}^m$ is the measurement operator and $\epsilon\in\mathbb{R}^m$ is noise. A common challenge is that A ill-conditioned or rank-deficient, making the inverse problem challenging due to the lack of a unique or stable solution. Traditional methods solve inverse problems by minimizing the sum of a measurement-consistency term and a handcrafted prior using an iterative algorithm. Modern approaches incorporate data-driven priors, either as fixed modules within classical iterative algorithms—such as in plug-and-play (PnP) priors [1, 2]—or as end-to-end learnable models, as in deep unrolling [3].

Deep equilibrium models (DEQ) formulate reconstruction as a fixed point of a learned operator [4, 5]. Unlike deep unrolling,

DEQ supports effectively infinite iterations while retaining memory efficiency and trainability via implicit differentiation [4]. Although PnP methods also yield fixed-point solutions [6], their operators are not learned end-to-end, limiting task-specific adaptability. DEQ overcomes this limitation and achieves state-of-the-art performance across a range of imaging inverse problems [5, 7, 8, 9].

A major limitation of end-to-end models like deep unrolling and DEQ is their reliance on paired training data. In many practical settings, such as medical or scientific imaging, ground truth signals are unavailable. Equivariant Imaging (EI) enables self-supervised training using only measurements by leveraging known symmetries in the signal set (e.g., rotations, translations) to define consistency-based losses [10].

Training DEQs under the EI framework can offer the best of both worlds: task-adapted models trained without requiring ground truths and the representational capacity of deep implicit networks. However, incorporating complex, transformation-based EI loss functions into DEQ training presents technical challenges due to the need for differentiating through the fixed point computations multiple times. Although Jacobian-free backpropagation [11] can avoid the complexity of implicit differentiation, it introduces approximation errors that can degrade trained model performance.

In this work, we show that a modular implementation of implicit differentiation can simplify training DEQ using complex loss functions, including those arising from EI. Although prior work has applied this modular implementation for supervised learning in code [5], there lacks a formal explanation or application to more complex loss functions. We hope that our formalization clarifies the use of implicit differentiation in practice and shows its useful application to self-supervised settings. We further show that the resulting DEQ trained via EI exhibits equivariance, suggesting that it implicitly learns a proximal map corresponding to a symmetry-invariant prior function. In summary, we make the following contributions.

- Modular Implicit Differentiation: We show that backpropagation for DEQ using implicit differentiation can be implemented in modular fashion, enabling training with complex loss functions involving multiple passes through the DEQ.
- Implicit Differentiation vs. Jacobian-Free Backpropagation:
 Our experimental results show that DEQs trained using implicit
 differentiation outperform those trained using Jacobian-free back propagation for both supervised and EI loss functions.
- Equivariant DEQ: We show that DEQs trained with EI are equivariant, indicating that the learned operator behaves as the proximal map of an invariant prior.

2 BACKGROUND

2.1 Equivariant Imaging

In supervised learning, we seek a reconstruction map f_{θ} parameterized by θ such that the reconstruction approximates the ground truth: $f_{\theta}(y) := \widehat{x}(\theta) \approx x$. We focus on learned reconstruction maps in this paper and often drop θ , writing simply \widehat{x} . Given a paired dataset $\{(x_i, y_i)\}_{i=1}^N$, supervised training requires minimizing the objective

$$\mathcal{L}_{SUP}(\theta) = \sum_{i} \ell_{SUP}(f_{\theta}(y_i), x_i), \tag{2}$$

with respect to θ , where ℓ_{SUP} is a supervised loss function for an individual sample, and $\mathcal{L}_{\text{SUP}}(\theta)$ is the corresponding total loss.

Given the challenge of acquiring ground truth x in many settings, the EI framework proposes end-to-end training of a reconstruction map f_{θ} using only measurement data [10]. Suppose the signals of interest belong to a set $\mathcal X$ that is invariant under a group of unitary transformations $\mathcal G$, i.e., $T_gx\in\mathcal X$ for any $x\in\mathcal X$ and any $g\in\mathcal G$. Then, EI proposes training f_{θ} by minimizing the objective

$$\mathcal{L}_{EI}(\theta) = \sum_{i=1}^{N} \ell_{MC}(\widehat{x}_i, y_i) + \alpha \sum_{i=1}^{N} \sum_{g \in \mathcal{G}} \ell_{EQ}(T_g \widehat{x}_i, f_{\theta}(AT_g \widehat{x}_i)),$$
(3)

where $\widehat{x}_i(\theta) = f_{\theta}(y_i)$, and $\alpha > 0$ is a hyperparameter. The loss ℓ_{MC} enforces measurement consistency, such as $\|Ax-y\|_2^2$, while ℓ_{EQ} ensures equivariance of the system $f_{\theta} \circ A$ to the group \mathcal{G} . When A is not equivariant to \mathcal{G} , applying $\{T_g\}_{g \in \mathcal{G}}$ introduces virtual measurement operators $\{AT_g\}_{g \in \mathcal{G}}$ to the training and enables f_{θ} to reconstruct signals outside the range space of A [10].

2.2 Deep Equilibrium Models

A DEQ is a neural network where the output is a fixed point of a learnable operator [4]. Given a measurement y from the forward model (1), a DEQ returns a reconstruction $\widehat{x}(\theta)$ satisfying

$$\widehat{x} = F_{\theta}(\widehat{x}; y), \tag{4}$$

where F_{θ} is a learnable operator parameterized by θ . In the context of inverse problems, designing F_{θ} based on an iteration of a PnP method has been shown to improve the reconstruction accuracy [5]. For example, consider the measurement-consistency loss $\ell_{MC}(x,y) = \|Ax - y\|^2$ for the forward model (1). Using the PnP proximal gradient method [2] results in

$$F_{\theta}(x;y) = D_{\theta}(x - \eta \nabla_x \ell_{MC}(x,y)) \tag{5}$$

$$= D_{\theta}(x - \eta A^{\top}(Ax - y)), \tag{6}$$

where D_{θ} is the learnable module that replaces the fixed denoiser in PnP PGM, and $\eta > 0$ is a step size. The fixed point of F_{θ} can be

computed through fixed-point iterations or using acceleration techniques [4, 5] such as Broyden's method [12] or Anderson acceleration [13].

For a DEQ, $f_{\theta}(y) = \operatorname{Fix}_{\widehat{x}}\{F_{\theta}(\widehat{x};y)\}$, where $\operatorname{Fix}_{x}\{f(x)\}$ denotes the fixed point x^* satisfying $x^* = f(x^*)$. Training a DEQ in supervised fashion by minimizing (2) with a gradient based method is challenging, because backpropagation through fixed-point iterations typically incurs an intractably large memory footprint. To address this, we can exploit the fixed-point condition (4) to rewrite the gradient of a loss $\ell(\widehat{x})$ with respect to θ as

$$\frac{\partial \ell(\widehat{x})}{\partial \theta} = \frac{\partial \ell(\widehat{x})}{\partial \widehat{x}} \left(I - \frac{\partial F_{\theta}(x)}{\partial x} \Big|_{x=\widehat{x}} \right)^{-1} \frac{\partial F_{\theta}(\widehat{x})}{\partial \theta}, \tag{7}$$

where, for brevity, we drop y in $F_{\theta}(x;y)$ [4, 5]. Explicitly computing the inverse matrix in (7) is generally intractable for high-dimensional signals. Implicit differentiation (ID) and Jacobian-free backpropagation (JFB) are two main approaches to overcome this problem. In ID, the gradient computation is reformulated as solving an auxiliary fixed-point problem:

$$\frac{\partial \ell(\widehat{x})}{\partial \theta} = \operatorname{Fix}_{\beta} \left\{ \beta \frac{\partial \operatorname{F}_{\theta}(x)}{\partial x} \Big|_{x = \widehat{x}} + \frac{\partial \ell(\widehat{x})}{\partial \widehat{x}} \right\} \frac{\partial \operatorname{F}_{\theta}(\widehat{x})}{\partial \theta}, \quad (8)$$

which can be solved using fixed-point iteration methods such as Broyden's method [12] and Anderson acceleration [13].

With JFB, the inverse matrix term is entirely dropped and the resulting vector $\frac{\widetilde{\partial \ell}}{\partial \theta} := \frac{\partial \ell}{\partial \widehat{x}} \frac{\partial F_{\theta}(\widehat{x})}{\partial \theta}$, which is a descent direction for θ under certain conditions, is used for backpropagation instead of the true gradient [11]. However, as shown later in Table 1, we find that DEQs trained using JFB achieve less accurate reconstructions compared to ID-trained DEQs.

3 BACKPROPAGATION FOR DEQ

3.1 Difficulty in Training DEQ with EI

Training a DEQ $f_{\theta}(y) = \operatorname{Fix}_{\widehat{x}}\{F_{\theta}(\widehat{x};y)\}$ by minimizing the EI objective (3) is complicated by DEQ's fixed point computation and multiple passes through $f_{\theta}(y)$. Consider the equivariant loss $\ell_{\text{EQ}}(x_2, x_3)$, where $x_2 = T_g f_{\theta}(y)$ and $x_3 = f_{\theta}(Ax_2)$. The gradient of $\ell_{\text{EQ}}(x_2, x_3)$ with respect to θ is

$$\frac{\partial \ell_{\text{EQ}}}{\partial \theta} = \frac{\partial \ell_{\text{EQ}}}{\partial x_2} \frac{\partial x_2}{\partial \theta} + \frac{\partial \ell_{\text{EQ}}}{\partial x_3} \left(\frac{\partial x_3}{\partial \theta} + \frac{\partial x_3}{\partial x_2} \frac{\partial x_2}{\partial \theta} \right). \tag{9}$$

Each of the three terms involves a derivative of a DEQ fixed point with respect to θ . In principle, we could apply ID separately to each term by deriving the corresponding fixed-point equation, similarly to equation (8). However, as detailed in Section 3.2, the gradient computation for all terms can be implemented modularly, using the same core code, without needing to manually formulate and solve three distinct fixed-point subproblems.

3.2 Modular Implicit Differentiation

We can simplify ID for complex loss functions such as (3) by leveraging the fact that the vector-Jacobian product between an upstream gradient and the Jacobian of a DEQ's fixed point with respect to its parameters can be systematically reduced to a fixed-point equation. This result is formalized in the following proposition.

Proposition 1. The vector-Jacobian product between a row vector $g \in \mathbb{R}^{1 \times n}$ and a Jacobian $\partial \widehat{x} / \partial \theta \in \mathbb{R}^{n \times p}$ of a fixed point $\widehat{x} = F_{\theta}(\widehat{x})$ with respect to the parameters $\theta \in \mathbb{R}^n$ is

$$g\frac{\partial \widehat{x}}{\partial \theta} = \operatorname{Fix}_{\beta} \left\{ \beta \frac{\partial \operatorname{F}_{\theta}(x)}{\partial x} \Big|_{x=\widehat{x}} + g \right\} \frac{\partial \operatorname{F}_{\theta}(\widehat{x})}{\partial \theta}. \tag{10}$$

```
1 \# F(x, y) is the learnable operator.
  # solver(func) yields a fixed point x=func(x).
3
  def forward(y):
4
      with torch.no_grad():
5
          xhat = solver(lambda x: F(x, y))
6
      xhat = F(xhat, y)
      x2 = xhat.clone().detach().requires_grad_()
8
      Fx = F(x2, y)
      def backward_hook(grad):
10
          bstar = solver(lambda b:
11
              autograd.grad(Fx, x2, b)[0] + grad)
12
           return bstar
13
      xhat.register_hook(backward_hook)
14
      return xhat
```

Fig. 2. PyTorch implementation of DEQ forward pass and implicit differentiation, adapted from $[5]^2$. The fixed-point is computed in lines 3–4; the remaining lines implement ID. Lines 7-12 define backward_hook for backpropagating through the fixed point xhat given an upstream gradient grad. Line 6 performs an evaluation of F_{θ} so that $\partial F_{\theta}(\widehat{x})/\partial \theta$ is captured in the autograd graph.

We represent gradients as row vectors to avoid unnecessary transposes, simplifying notation. The standard ID formulation (8) is a direct consequence of Theorem 1 when $g=\partial\ell/\partial\widehat{x}$. This proposition enables a modular implementation of ID: any vector–Jacobian product involving the DEQ's output can be replaced with the fixed-point computation in (10), followed by a multiplication with $\partial F_{\theta}(\widehat{x})/\partial\theta$. The PyTorch implementation shown in Figure 2 directly realizes this computation.

Although this modular implementation of ID was previously used in code for supervised reconstruction with DEQs [5], to the best of our knowledge, Theorem 1 provides the first mathematical formalization of this technique, and our work is the first to apply it to the self-supervised EI setting.

4 EXPERIMENTS

We evaluate the performance of DEQs trained using the EI framework with ID against a range of reconstruction methods. These include DEQs trained with supervision, DEQs trained using JFB, as well as several baseline methods: deep unrolled models, U-Net refinement, PnP priors, and Regularization by Denoising (RED) [14].

4.1 Tasks

We consider two representative inverse problems: sparse-view computed tomography (CT) and accelerated magnetic resonance imaging (MRI). Both imaging systems follow the linear forward model in (1). For EI training, we define the transformation group $\mathcal G$ as rotations in 1-degree increments ($|\mathcal G|=360$) for both tasks. Since the forward operators for accelerated MRI and sparse-view CT are not equivariant to rotations, each AT_g has a different null-space, enabling learning without access to any ground truth. Each dataset is split into 90% for training and 10% for testing. We use the Deep Inverse library [15] for the implementation of measurement operators A and related operators such as pseudoinverses A^{\dagger} . We use TorchDEQ for the implementation of DEQs [16].

4.1.1 Sparse-view CT

The measurement operator A is the discrete Radon transform, subsampled over 50 projection angles uniformly spaced between 0° and 180° . We use the CT100 dataset [17], which consists of 100 CT images, each resized to size 128×128 . The forward model is assumed

to be noiseless ($\epsilon=0$). We found equivariance strength of $\alpha=100$ was best for all models based on hyperparameter search.

4.1.2 Accelerated MRI

The task is $8\times$ accelerated single-coil MRI. The measurement operator A is a subsampled 2D discrete Fourier transform with a fixed Gaussian mask. The mask fully samples low-frequency components and randomly samples high-frequency components based on a Gaussian distribution [18]. The real and complex parts of the measurements are fed to two channels for all models. Additive white Gaussian noise with standard deviation 0.05 is added to the measurements. The dataset consists of 199 knee scan slices with size 320×320 from the fastMRI dataset [19]. We used $\alpha=1$ for all MRI experiments based on hyperparameter search. Similar to CT, we found that the best α value didn't vary across U-Nets or DEQs.

4.2 Reconstruction Methods

DEQs, deep unrolling models, and the U-Net models are trained endto-end, while PnP prior and RED use a pre-trained denoiser without end-to-end training.

4.2.1 Deep Equilibrium Models

We use different iterative reconstruction methods as templates for the two tasks to demonstrate wide applicability of modular ID. For CT, we use RED as the template, resulting in the DE-Grad architecture [5]:

$$F_{\theta}(x) = x - \eta \nabla \ell_{MC}(x) - \eta(x - D_{\theta}(x)). \tag{11}$$

For MRI, we use PGM as the template, resulting the fixed-point operator defined in (5), i.e., the DE-Prox architecture [5]. For both DEQs, the learnable module D_{θ} is a residual U-Net denoiser [20], whose initial weights are pretrained on the BSD500 dataset [21]. To ensure that F_{θ} is contractive and admits a fixed point, we follow standard practice by applying spectral normalization or weight normalization [22] and using group normalization layers [23].

4.2.2 Deep Unrolling

We implement deep unrolled models based on the iterative algorithm corresponding to each task: RED for CT and PGM for MRI; unrolled PGM is also known as LISTA [3]. Model weights in all iterations are shared to keep the number of parameters consistent with DEQs. The deep unrolled models use the same initial U-Net denoiser as our DEQ experiments.

4.2.3 U-Net Refinement

We include a simple U-Net baseline reconstruction that refines the pseudoinverse solution, i.e., $f_{\theta}(y) = D_{\theta}(A^{\dagger}y)$, following experiments in [10].

4.2.4 PnP / RED

These classical iterative methods use pretrained denoisers without end-to-end training. We use RED [14] for CT and PnP PGM [2] for MRI. Both use a DnCNN denoiser [24] with weights from the Deep Inverse library [15]. We use DnCNN instead of U-Net as we found that U-Net performs poorly as a denoiser and yields worse reconstruction when used in PnP and RED.

4.3 Results

4.3.1 ID yields better models than JFB

As shown in Table 1, DEQs trained with ID consistently outperform those trained with JFB. Although JFB offers computational convenience, the lack of exact gradient information leads to suboptimal convergence and inferior reconstruction quality.

¹Adapted from the code in Gilton et al.

Task	Method	DEQ		U-Net	Unrolled			PnP/RED	
		ID	JFB	$A^{\dagger}y$	1-Layer	3-Layer	5-Layer	7-Layer	DnCNN
MRI	Supervised Self-Supervised	32.61 31.34	32.51 29.39	30.587 28.02	29.16 27.35	29.45 27.56	29.33 27.12	29.57 27.24	25.07
CT	Supervised Self-Supervised	36.77 35.41	32.80 33.52	36.33 34.03	35.14 31.73	34.57 32.01	34.99 32.34	35.80 <u>34.66</u>	31.90

Table 1. Test PSNR. The best result is in bold and the second best is underlined. DEQ trained with ID outperforms U-Net and DEQ with JFB. Despite having access to no ground truth data, EI performance is close to supervised.

4.3.2 EI performance is close to supervised

Using ID, DEQs trained with EI attains a PSNR within 1.3 dB of that achieved by supervised training. This result demonstrates the effectiveness of EI as a self-supervised approach for training powerful reconstruction models when ground truth is unavailable. Additionally, both DEQ and U-Net models trained using EI have higher test PSNR than denoiser-based methods like PnP and RED.

4.3.3 DEQ has the strongest performance

DEQ-based methods achieve the strongest overall performance across both tasks, outperforming unrolled networks, U-Net refinement, and PnP/RED. These results highlight the strength of DEQ in capturing the structure of inverse problems more effectively than deep unrolling or PnP/RED.

5 DISCUSSION

5.1 Imaging Pipeline is Equivariant

	Method	Equivariant Imaging	Supervised
MRI	DEQ	34.64 ± 2.449	34.66 ± 2.340
MRI	U-Net	28.01 ± 1.311	25.62 ± 1.244
CT	DEQ	47.57 ± 1.268	39.24 ± 2.734
CT	U-Net	42.55 ± 1.449	36.48 ± 1.989

Table 2. Equivariance error of imaging pipeline $f_{\theta} \circ A$, quantified by PSNR of the difference between $f_{\theta}(AT_gx)$ and $T_gf_{\theta}(Ax)$.

If the signal set is invariant under a group of transformations \mathcal{G} , then it is natural to expect the entire measurement-reconstruction system $f_{\theta} \circ A$ to be equivariant with respect to \mathcal{G} [10]. For instance, a reconstruction from an MRI scan of a rotated patient should correspond to the rotation of the original reconstruction.

Results in Table 2 demonstrates this system equivariance property. We quantify the equivariance of $f_{\theta} \circ A$ by computing the average difference between $f_{\theta}(AT_gx)$ and $T_gf_{\theta}(Ax)$ across test set images x, reporting the result in terms of PSNR (referred to as *equivariance error*). While all ngles are used during training, we only choose T_g to be a 90° counterclockwise rotation to avoid aliasing edge artifacts.

EI-trained models have significantly higher equivariance error than those from supervised training. We attribute this observation to the training data, which are not augmented by rotated images, whereas EI implicitly augments rotated images during training.

5.2 EI-trained DEQ Operator is Equivariant

Training DEQs using the EI framework also reveals a deeper structural property: the learned operator F_{θ} becomes equivariant to the

	EI	Supervised	Initialization
MRI	39.96 ± 2.333	32.59 ± 2.062	37.50 ± 0.564
CT	52.44 ± 1.412	46.75 ± 2.056	33.94 ± 0.768

Table 3. Equivariance error of DEQ operator F_{θ} , quantified by PSNR of the difference between $T_g F_{\theta}(x, Ax)$ and $F_{\theta}(T_g x, AT_g x)$. Initialization refers to a DEQ where D_{θ} is the pretrained denoiser used at the start of training.

transformation group \mathcal{G} . As shown in Table 3, DEQs trained with EI exhibit significantly stronger equivariance than those trained with standard supervised learning. This is quantified by the PSNR of the difference between T_g $F_{\theta}(x,Ax)$ and $F_{\theta}(T_gx,AT_gx)$ averaged over test images. Again, we evaluate equivariance T_g with a 90° rotation to avoid edge artifacts.

This result suggests that the DEQ's learnable module D_{θ} approximates the proximal map of a \mathcal{G} -invariant prior function, as the proximal map of an invariant function is equivariant under unitary group actions [25]. The equivariant loss ℓ_{EQ} in the EI objective (3) is invariant to \mathcal{G} when averaged over group elements $g \in \mathcal{G}$, further supporting the interpretation that the DEQ implicitly learns an invariant prior.

This observation highlights a deeper connection between explicit regularization and learned reconstruction maps, which is a major theoretical question. Prior works have explored this relationship in various contexts [14, 26, 27, 28, 29].

6 CONCLUSION

We formalize a modular implementation of implicit differentiation for training DEQs and demonstrate the performance gain of training DEQs with implicit differentiation when compared to Jacobian-free backpropagation and other reconstruction methods. We also show that the resulting EI-trained operator in DEQ is equivariant, suggesting that DEQ implicitly learns an invariant prior function.

Given the superior reconstruction quality of DEQs, developing more robust and efficient methods for training DEQs, especially in self-supervised settings, remains a critical direction for future work, as it unlocks the potential to use DEQs in domains where ground truth data are limited or unavailable. Although our results suggest that DEQ implicitly learns an invariant prior function, our evidence is not conclusive. A rigorous characterization of the implicit prior is another future direction.

7 REFERENCES

[1] Singanallur V Venkatakrishnan, Charles A Bouman, and Brendt Wohlberg, "Plug-and-play priors for model based reconstruction," in 2013 IEEE global conference on signal and information processing. IEEE, 2013, pp. 945–948.

- [2] Ulugbek S. Kamilov, Hassan Mansour, and Brendt Wohlberg, "A Plug-and-Play Priors Approach for Solving Nonlinear Imaging Inverse Problems," *IEEE Signal Process. Lett.*, vol. 24, no. 12, pp. 1872–1876, Oct. 2017.
- [3] Karol Gregor and Yann LeCun, "Learning fast approximations of sparse coding," in *Proc. Int. Conf. Mach. Learn.*, 2010, pp. 399–406.
- [4] Shaojie Bai, J. Zico Kolter, and Vladlen Koltun, "Deep equilibrium models," in *Adv. Neural Inf. Process. Syst.*, H. Wallach, H. Larochelle, A. Beygelzimer, F. d'Alché-Buc, E. Fox, and R. Garnett, Eds. 2019, vol. 32, Curran Associates, Inc.
- [5] Davis Gilton, Gregory Ongie, and Rebecca Willett, "Deep equilibrium architectures for inverse problems in imaging," *IEEE Trans. Comput. Imaging*, vol. 7, pp. 1123–1133, 2021.
- [6] Ernest Ryu, Jialin Liu, Sicheng Wang, Xiaohan Chen, Zhangyang Wang, and Wotao Yin, "Plug-and-play methods provably converge with properly trained denoisers," in *Proc. Int. Conf. Mach. Learn.* 2019, pp. 5546–5557, PMLR.
- [7] Alper Güngör, Baris Askin, Damla Alptekin Soydan, Can Bariş Top, Emine Ulku Saritas, and Tolga Çukur, "Deqmpi: A deep equilibrium reconstruction with learned consistency for magnetic particle imaging," *IEEE Trans. Medical Imaging*, vol. 43, no. 1, pp. 321–334, 2024.
- [8] Kerstin Hammernik, Thomas Küstner, Burhaneddin Yaman, Zhengnan Huang, Daniel Rueckert, Florian Knoll, and Mehmet Akçakaya, "Physics-driven deep learning for computational magnetic resonance imaging: Combining physics and machine learning for improved medical imaging," *IEEE Signal Process. Mag.*, vol. 40, no. 1, pp. 98–114, 2023.
- [9] Yaping Zhao, Siming Zheng, and Xin Yuan, "Deep equilibrium models for snapshot compressive imaging," *Proc. AAAI Conf. Artif. Intell.*, vol. 37, no. 3, pp. 3642–3650, 2023.
- [10] Dongdong Chen, Julian Tachella, and Mike E. Davies, "Equivariant Imaging: Learning Beyond the Range Space," Proc. IEEE Int. Conf. Comput. Vis., Oct. 2021.
- [11] Samy Wu Fung, Howard Heaton, Qiuwei Li, Daniel McKenzie, Stanley Osher, and Wotao Yin, "Jfb: Jacobian-free back-propagation for implicit networks," *Proc. AAAI Conf. Artif. Intell.*, vol. 36, no. 6, pp. 6648–6656, 2022.
- [12] Charles G Broyden, "A class of methods for solving nonlinear simultaneous equations," *Mathematics of computation*, vol. 19, no. 92, pp. 577–593, 1965.
- [13] Homer F. Walker and Peng Ni, "Anderson Acceleration for Fixed-Point Iterations," *SIAM J. Numer. Anal.*, vol. 49, no. 4, pp. 1715–1735, July 2011.
- [14] Yaniv Romano, Michael Elad, and Peyman Milanfar, "The little engine that could: Regularization by denoising (red)," SIAM J. Imaging Sci., vol. 10, no. 4, pp. 1804–1844, 2017.
- [15] Julián Tachella, Matthieu Terris, Samuel Hurault, Andrew Wang, Dongdong Chen, Minh-Hai Nguyen, Maxime Song, Thomas Davies, Leo Davy, Jonathan Dong, et al., "Deepinverse: A python package for solving imaging inverse problems with deep learning," arXiv preprint arXiv:2505.20160, 2025.
- [16] Zhengyang Geng and J. Zico Kolter, "TorchDEQ: A Library for Deep Equilibrium Models," Oct. 2023.
- [17] Kenneth Clark, Bruce Vendt, Kirk Smith, John Freymann, Justin Kirby, Paul Koppel, Stephen Moore, Stanley Phillips, David Maffitt, Michael Pringle, Lawrence Tarbox, and Fred Prior, "The cancer imaging archive (TCIA): maintaining and operating a public information repository," *J. Digit. Imaging*, vol. 26, no. 6, pp. 1045–1057, Dec. 2013.
- [18] Jo Schlemper, Jose Caballero, Joseph V. Hajnal, Anthony N.

- Price, and Daniel Rueckert, "A deep cascade of convolutional neural networks for dynamic mr image reconstruction," *IEEE Trans. Medical Imaging*, vol. 37, no. 2, pp. 491–503, 2018.
- [19] Jure Zbontar, Florian Knoll, Anuroop Sriram, Tullie Murrell, Zhengnan Huang, Matthew J. Muckley, Aaron Defazio, Ruben Stern, Patricia Johnson, Mary Bruno, Marc Parente, Krzysztof J. Geras, Joe Katsnelson, Hersh Chandarana, Zizhao Zhang, Michal Drozdzal, Adriana Romero, Michael Rabbat, Pascal Vincent, Nafissa Yakubova, James Pinkerton, Duo Wang, Erich Owens, C. Lawrence Zitnick, Michael P. Recht, Daniel K. Sodickson, and Yvonne W. Lui, "fastMRI: An Open Dataset and Benchmarks for Accelerated MRI," arXiv, Nov. 2018
- [20] Olaf Ronneberger, Philipp Fischer, and Thomas Brox, "U-net: Convolutional networks for biomedical image segmentation," in *Proc. Int. Conf. Med. Image Comput. Comput.-Assist. Interv.* Springer, 2015, pp. 234–241.
- [21] D. Martin, C. Fowlkes, D. Tal, and J. Malik, "A database of human segmented natural images and its application to evaluating segmentation algorithms and measuring ecological statistics," in *Proc. 8th Int'l Conf. Computer Vision*, July 2001, vol. 2, pp. 416–423.
- [22] Tim Salimans and Durk P Kingma, "Weight normalization: A simple reparameterization to accelerate training of deep neural networks," Adv. Neural Inf. Process. Syst., vol. 29, 2016.
- [23] Yuxin Wu and Kaiming He, "Group normalization," in *Proc. Eur. Conf. Comput. Vis.*, 2018, pp. 3–19.
- [24] Kai Zhang, Wangmeng Zuo, Yunjin Chen, Deyu Meng, and Lei Zhang, "Beyond a gaussian denoiser: Residual learning of deep cnn for image denoising," *IEEE Trans. Image Process.*, vol. 26, no. 7, pp. 3142–3155, 2017.
- [25] Elena Celledoni, Matthias J Ehrhardt, Christian Etmann, Brynjulf Owren, Carola-Bibiane Schönlieb, and Ferdia Sherry, "Equivariant neural networks for inverse problems," *Inverse Problems*, vol. 37, no. 8, pp. 085006, 2021.
- [26] Zihao Zou, Jiaming Liu, Brendt Wohlberg, and Ulugbek S. Kamilov, "Deep equilibrium learning of explicit regularization functionals for imaging inverse problems," *IEEE Open J. Signal Process.*, vol. 4, pp. 390–398, 2023.
- [27] Samuel Hurault, Arthur Leclaire, and Nicolas Papadakis, "Gradient step denoiser for convergent plug-and-play," arXiv preprint arXiv:2110.03220, 2021.
- [28] Alexis Goujon, Sebastian Neumayer, Pakshal Bohra, Stanislas Ducotterd, and Michael Unser, "A neural-network-based convex regularizer for inverse problems," *IEEE Trans. Comput. Imaging*, vol. 9, pp. 781–795, 2023.
- [29] Zhenghan Fang, Sam Buchanan, and Jeremias Sulam, "What's in a prior? learned proximal networks for inverse problems," arXiv preprint arXiv:2310.14344, 2023.